POLITECNICO DI TORINO
Repository ISTITUZIONALE

Ultimate shear of RC beams with corroded stirrups and strengthened with FRP

Original
Ultimate shear of RC beams with corroded stirrups and strengthened with FRP / Spinella, Nino; Colajanni, Piero; Recupero, Antonino; Tondolo, Francesco. - In: BUILDINGS. - ISSN 2075-5309. - 9:2(2019), p. 34. [10.3390/buildings9020034]

Availability:
This version is available at: 11583/2732963 since: 2019-05-11T13:29:15Z

Publisher:
MDPI AG

Published
DOI:10.3390/buildings9020034

Terms of use:

This article is made available under terms and conditions as specified in the corresponding bibliographic description in the repository

Publisher copyright

(Article begins on next page)

02 May 2024

buildings

MDPI

Article

Ultimate Shear of RC Beams with Corroded Stirrups and Strengthened with FRP

Nino Spinella [1,*], Piero Colajanni [2], Antonino Recupero [1] and Francesco Tondolo [3]

[1] Department of Engineering, Università di Messina, 98166 Messina, Italy; antonino.recupero@unime.it
[2] Department of Engineering, Università di Palermo, 90128 Palermo, Italy; piero.colajanni@unipa.it
[3] Department of Structural, Geotechnical and Building Engineering, Politecnico di Torino, 10129 Torino, Italy; francesco.tondolo@polito.it
* Correspondence: nino.spinella@unime.it; Tel.: +39-090-397-7161

Received: 26 December 2018; Accepted: 24 January 2019; Published: 29 January 2019

Abstract: Transverse reinforcement plays a key role in the response behavior of reinforced concrete beams. Therefore, corrosion of steel stirrups may change the failure mode of elements from bending to shear, leading to a brittle and catastrophic crisis. It is important to strengthen reinforced concrete beams with corroded stirrups to enhance the shear resistance. This paper presents a formulation, based on the modified compression field theory, to estimate the ultimate shear of reinforced concrete beams strengthened with FRP, because of stirrup corrosion. The detrimental effect of corrosion on steel stirrup yield strength was taken into account by introducing an empirical decay law. The effective strain of FRP reinforcement was adequately evaluated by considering both debonding and tensile stress rupture. The proposed model was validated against collected experimental results, showing a good ability to evaluate shear strength. Moreover, a numerical analysis was carried out to highlight the role of the key parameters predicting the ultimate shear.

Keywords: corrosion; stirrups; shear; FRP; MCFT; reinforced concrete; beams; parametric analysis

1. Introduction

The decay of structural performance occurs in many existing reinforced concrete (RC) structures due to reinforcement corrosion. It leads to the loss of the cross-sectional area of the steel bars, cracking of the concrete cover, and a damaging effect on the bond between steel bars and concrete [1–5].

In this scenario, premature failure can occur. To avoid this, retrofitting of structures is necessary in order to ensure the safety and serviceability of RC structures damaged by corrosion [6–9].

Due to their position, stirrups are vulnerable to chloride-induced corrosion, and corrode more rapidly than longitudinal steel bars, also because of their smaller diameter [10].

Stirrup corrosion is strictly related to concrete cover cracking. When the degree of corrosion is not enough to induce cracking, the shear behavior is not significantly degraded. By contrast, the start of cracking of the concrete cover, related to the increase in the degree of stirrup corrosion, leads to a proportional decay of the shear strength of the RC beam.

In the literature, several models have alternatively been proposed to evaluate the shear strength of RC beams with corroded stirrups [11–14] or reinforced with composites [15–18].

Conversely, few models have been presented to evaluate the shear strength of RC beams which were initially subject to corrosion of the reinforcements, and were subsequently strengthened with composites [6,8,19].

This research work aims to contribute to an understanding of the shear failure mechanism of RC beams with corroded stirrups and strengthened in shear with FRP sheets. The proposed model, based on the Modified Compression Field Theory (MCFT) [20], considers the influence of both stirrup corrosion and FRP transverse reinforcement on the ultimate shear of RC beams.

The effective strain of FRP ($_{fe}$) at the Ultimate Limit State (ULS) was estimated by considering both the debonding and tensile stress rupture of composite sheets, as suggested by Chen and Teng [21,22].

The detrimental effect of corrosion on the yield strength of steel stirrups was assessed by an empirical law that was recently suggested by the same authors [2,12].

Finally, the proposed formulation of ultimate shear was verified against available experimental data obtained by other researchers, and a sensitivity analysis of the parameters involved was carried out.

2. Effective Strain of FRP at ULS

The contribution of FRP at ultimate shear can be estimated as follows:

$$V_f = A_{fv} f_{fe} cot\theta \quad (1)$$

where A_{fv} is the area of transverse FRP reinforcement; $f_{fe} = E_{fv}\, \varepsilon_{fe} = E_{fv}\, R_f\, \varepsilon_{fu}$ is the FRP stress at ULS, with E_{fv} the Elastic modulus of FRP; ε_{fu} is the ultimate strain of FRP; and R_f is the effectiveness factor of FRP (≤ 1); and θ the strut inclination angle with respect to the longitudinal axis of the beam.

The effectiveness of FRP strengthening at ultimate shear is dependent on the failure mode achieved (debonding or rupture of FRP sheets). In turn, the stress of FRP at failure is also governed by the arrangement of the composite reinforcement (Figure 1).

If the FRP sheets are on two sides [Side-bonding (S)] of the cross-section, then the main crisis mode is debonding of FRP. U-shaped (U) strengthening may be, alternatively, governed by either of the two failure modes (either rupture or debonding). When the FRP sheet is completely wrapped (C) around the beam cross-section, the rupture of FRP sheets governs failure.

Therefore, at least two different calculation models of the effectiveness strain should be adopted.

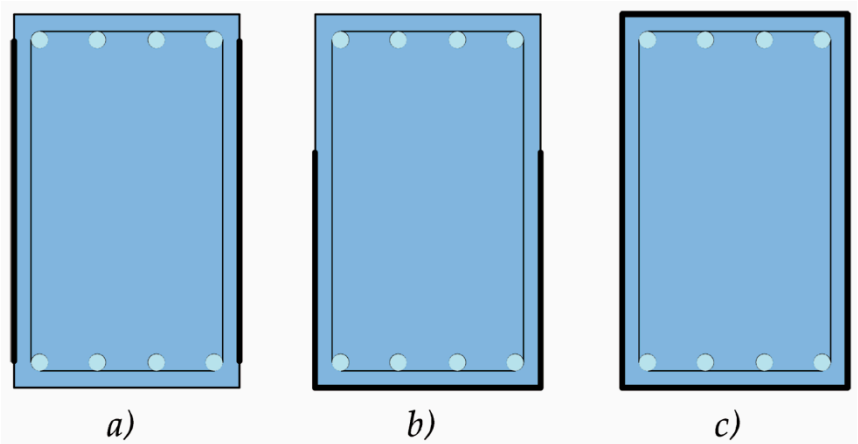

Figure 1. FRP sheets detailing: (**a**) Side-Bonding (S); (**b**) U-shaped (U); and (**c**) Completely-Wrapped (C).

2.1. Rupture of FRP

The axial strain in the FRP can be assumed in the order of proportionality to the shear critical crack width, and a linear distribution of FRP strain may be used [15]. Thus, the effectiveness factor for rupture (R_{fr}) can be expressed as [22]:

$$R_{fr} = \left[1 + \left(h - d_f\right)/jd\right]/2 \tag{2}$$

where d_f is the height of the FRP reinforcement and jd is the inner lever arm.

2.2. Debonding of FRP

When the FRP amount and the bond length are not adequately designed with respect to the tensile and the bond strength of concrete, or the adhesive-to-concrete bond strength is not sufficient, debonding failure of FRP may occur.

In this case, the contribution of FRP reinforcement to the ultimate shear of the beam is governed by the bond between FRP and surrounding concrete. The maximum variable stress in the FRP along the bond length ($\sigma_{f,max}$) can be evaluated as:

$$\sigma_{f,max} = 0.427\beta_w\beta_L\sqrt{\frac{E_f\sqrt{f_c}}{t_f}} \leq E_f\varepsilon_{fu} \tag{3}$$

where β_w is the coefficient of the FRP-to-concrete width ratio and β_L is the bond length coefficient.

These values are a function of the normalized maximum bond length (λ); the effectiveness factor for debonding (R_{fd}) can be expressed as [21]:

$$R_{fd} = \frac{\sigma_{f,max}}{E_f\varepsilon_{fu}}\begin{cases} \frac{2}{\pi\lambda}\frac{1-cos\frac{\pi\lambda}{2}}{sin\frac{\pi\lambda}{2}} & for \quad \lambda < 1 \\ 1 - \frac{\pi-2}{\pi\lambda} & for \quad \lambda \geq 1 \end{cases} \tag{4}$$

3. Empirical Relationship for the Yield Strength of Corrosion-Damaged Steel Stirrups

The corrosion process deeply influences the mechanical properties of the steel rebar. Specifically, the steel yield strength is strictly related to the ultimate capacity of the structural element.

Therefore, a linear decay law, as suggested by Cairns et al. [23], was slightly modified. The linear dependency between the yield strength of un-corroded and corroded steel rebar is very handy from a design point of view, avoiding introducing any complication in the calculation procedure.

In a previous research work by the same authors [12], a database was collected to calculate the negative slope (α_y) of a linear equation, in the following form:

$$f_{y,c}/f_y = 1 - \alpha_y Q_c \tag{5}$$

where $f_{y,c}$ and f_y are the yield strength of the corroded and un-corroded steel rebars respectively, and $Q_c = (A_{sv,c} - A_{sv})/A_{sv}$ is the average corrosion degree, $A_{sv,c}$ and A_{sv} being the area of transversal reinforcement in the corroded and un-corroded configuration, respectively.

Five campaigns (230 specimens) of tensile tests on artificially corroded steel rebars [24–28] were considered. Only the specimens tested by Zhang et al. [25] were obtained from both the natural corrosion process and an accelerated corrosion process.

The test results showed that the mechanical properties degraded with an increase in the degree of corrosion. Moreover, the detrimental effects were greater when the diameter of the rebar was smaller [2,27].

In Figure 2, the experimental reduction of the yield capacity ratio of the corrosion-damaged steel versus the average cross-sectional loss of the corroded tension rebar is shown. In addition, adopting an the empirical coefficient α_y = 0.0094, obtained by regression analysis, Equation (5) is also plotted. The slope of the degradation trend model of the steel yield ratio is close to the analogous value observed in their experiments by Zhu et al. (α_y = 0.01) [29], and smaller than the value proposed by Imperatore et al. (α_y = 0.0151) [28].

The corrosion process deteriorates the bond between the stirrups and the surrounding concrete; however, it only causes a minor reduction in the shear strength, making it possible to ignore bond deterioration [8,30]. In any case, the retrofitting of damaged-corrosion beam can only improve the bond strength.

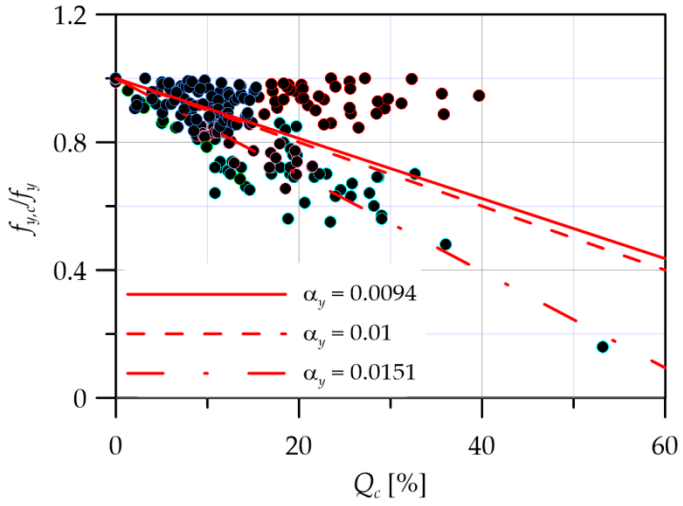

Figure 2. Experimental yield capacity ratio versus average corrosion degree of corroded steel rebar.

4. Analytical Model for the Ultimate Shear of Corrosion-Damaged Steel Stirrups Strengthened with FRP

Several models, also based on the MCFT equations, have been proposed in the literature to evaluate the shear-displacement curve of RC beams with and without FRP reinforcement [31–34].

The shear crack inclination, the crack width, and the effective strains are generally missing or difficult to measure in several experimental campaigns as extensive local instrumentation or advanced imaging techniques are required. Hence, Rousakis et al. [35] used the MCFT to calculate consistent average values for crucial shear-capacity related parameters. However, the MCFT makes it possible to take into account the interaction between the different contributions (concrete, stirrups, and FRP) to the ultimate shear.

Colalillo and Sheikh [31], suitably adapting the Uniaxial Shear-Flexural Model (USFM) for RC columns introduced by Mostafaei and Vecchio [32], presented an analytical method to predict the shear-deformation response of slender RC beams strengthened with FRP.

However, the USFM requires the assumption of a constant value for the strut strain, set equal to the average value of concrete uniaxial compression strains corresponding to the resultant forces of the concrete stress blocks between two different cross-sections [32].

In a different way, for RC beams reinforced in shear with FRP, the average principal compressive strain (ε_2) was taken as half of the uniaxial compressive strain at the maximum moment location, multiplied by the compression softening coefficient, and evaluated as the strain (ε_t) corresponding to the resultant compressive force (C) [31]. It follows that an accurate representation of the softening of the concrete compressive strain and stress is essential in calculating the ultimate shear [36].

In the presented formulation, it was assumed that the FRP at ULS had reached its effective strain, and the principal compressive strain was calculated as suggested by Colalillo and Sheikh [31]. Unlike the other two formulations considered, in this case, the flexural model was not separated from the shear one.

A sectional analysis was used to solve the shear model, while the classical flexural equations were applied to verify the compatibility conditions of the considered beam cross-section (Figure 3).

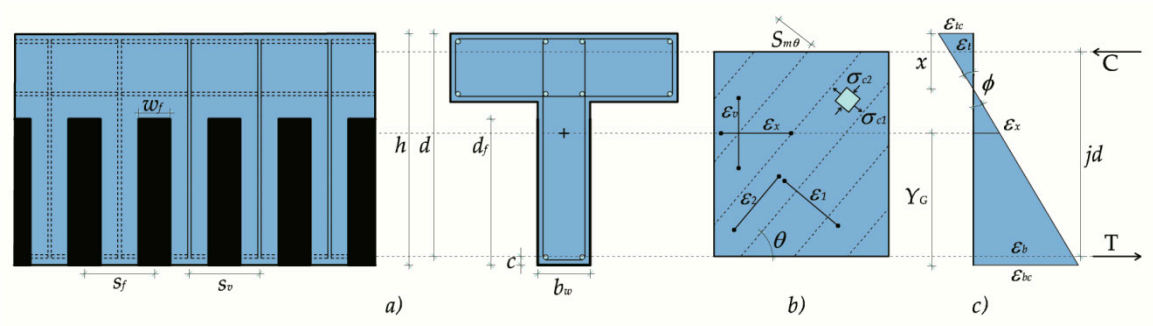

Figure 3. (**a**) Lateral view and cross-section of the RC beam strengthened with FRP. (**b**) Shear and (**c**) flexural model at ULS.

4.1. Shear Model

4.1.1. Equilibrium Equations

The equilibrium conditions of MCFT at ULS require that:

$$\sigma_{cv} = \sigma_{c1} - \tau / cot\theta \tag{6}$$

$$\sigma_{c2} = \sigma_{c1} - \tau \left(1/cot\theta + cot\theta\right) \tag{7}$$

where σ_{cv} is the concrete stress in the transverse direction; σ_{c1} and σ_{c2} are the concrete principal tensile and compressive stresses, respectively; and $\tau = V/(b_w\, d)$ is the ultimate shear stress.

The equilibrium equation along the vertical direction makes it possible to obtain the following expression of the clamping stress (σ_v):

$$\sigma_v = \sigma_{cv} + \rho_{sv,c}\sigma_{sv,c} + \rho_{fv}f_{fe} \tag{8}$$

where $\rho_{sv,c} = A_{sv,c}/(b_w\, s_v)$ is the geometrical ratio of corroded steel transverse reinforcement, with s_v spacing of stirrups; $\sigma_{sv,c}$ is the stress of the corroded stirrups; and $\rho_{fv} = A_{fv}/(b_w\, s_f)$ is the geometrical ratio of FRP reinforcement.

Taking the clamping stress to zero and substituting the Equation (8) into Equation (6) and rewriting Equation (8), the following relationships were derived:

$$\tau = \left(\sigma_{c1} + \rho_{sv,c}\sigma_{sv,c} + \rho_{fv}f_{fe}\right)\, cot\theta \tag{9}$$

$$\tau = (\sigma_{c1} - \sigma_{c2})cot\theta / \left(1 + cot^2\theta\right) \tag{10}$$

As the underlying model is the same, Equations (9) and (10) lead to an identical result. The corresponding inclination of the strut or the shear critical crack angle respectively can be calculated by equating the two expressions of the ultimate shear stress:

$$cot^2\theta = \frac{-\sigma_{c2} - \left(\rho_{sv,c}\sigma_{sv,c} + \rho_{fv}f_{fe}\right)}{\sigma_{c1} + \left(\rho_{sv,c}\sigma_{sv,c} + \rho_{fv}f_{fe}\right)} \tag{11}$$

Equation (11) represents a generalized form ($\sigma_{c1} > 0$ and $\rho_{fv}f_{fe} > 0$) of the strut angle inclination in the context of limit analysis [37], also being the basis of the ultimate shear formula proposed by several codes [38,39].

4.1.2. Compatibility Conditions

As suggested by Bentz et al. [40], the principal tensile strain at ULS can be calculated as a function of the longitudinal strain (ε_x), the principal compressive strain and the crack angle:

$$\varepsilon_1 = \varepsilon_x + (\varepsilon_x - \varepsilon_2)cot^2\theta \quad (12)$$

Therefore, calculating the flexural strain slope at ULS (ϕ) requires the estimation of both longitudinal strains ε_x and ε_t. Thus, it is possible to calculate $\varepsilon_2 = \varepsilon_t\eta/2$, where η is the compression softening factor.

4.1.3. Constitutive Laws

The stress-strain relationship of the compressive concrete in a diagonally-cracked web depends on the principal strains. Neglecting the confinement effects due to the transversal reinforcement [41], the following equations were used [20]:

$$\sigma_{c2} = f_{ce}\left[2\left(\frac{\varepsilon_2}{\varepsilon_{c0}}\right) - \left(\frac{\varepsilon_2}{\varepsilon_{c0}}\right)^2\right] \quad (13)$$

$$\eta = \frac{f_{ce}}{f_c} = \frac{1}{0.8 + 170\,\varepsilon_1} \leq 1 \quad (14)$$

where f_{ce} is the compressive strength of the diagonally cracked concrete, which decreases with the increase in the principal tensile strain (ε_1), and ε_{c0} is the strain at peak stress in the concrete (f_c).

Cracked concrete was still assumed to carry tensile stress due to tension stiffening mechanism. The interaction between the steel rebar and surrounding concrete may be described by the following equation [20]:

$$\sigma_{c1} = \frac{f_{ct}}{1 + \sqrt{500\,\varepsilon_1}} \quad (15)$$

where $f_{ct} = 0.33\,f_c{}^{0.5}$ is the concrete tensile strength.

The contribution of the principal tensile stress (σ_{c1}) to the ultimate shear must be limited by the capacity of the member to transmit forces across the crack. This is obtained by the equilibrium of local forces across the crack in the transverse directions:

$$\sigma_{c1,max} = \tau_i / cot\theta + \rho_{sv,c}\left(f_{yv,c} - \sigma_{sv,c}\right) \quad (16)$$

where τ_i is the local shear stress on the crack surface:

$$\tau_i = \frac{0.18\sqrt{f_c}}{0.31 + \frac{24w}{d_g + 16}} \quad (17)$$

where d_g is the maximum coarse aggregate size (in mm); and $w = \varepsilon_1\,S_{m\theta}$ is the average crack width (in mm).

The residual steel reinforcement stresses at the crack are taken as zero if the yield stress is reached ($\sigma_{sv,c} = f_{yv,c}$). This condition was not always satisfied, because the average vertical strain (ε_v) at ULS was set equal to the effective strain of FRP, and it can be less than the yield strain of the corroded steel stirrups.

The average diagonal crack spacing, $S_{m\theta} = 1/(sin\theta/S_{ml} + cos\theta/S_{mv})$, depends on the average crack spacing in the two orthogonal directions S_{ml} and S_{mv}. They were assumed to be equal to the stirrup spacing and the effective depth (d) of the cross-section, respectively [40].

4.2. Flexural Model

As mentioned, the flexural strain slope at ULS (ϕ) must satisfy the longitudinal equilibrium ($F_x = C + T = 0$) [42].

The longitudinal strains at compressive and tensile resultant force levels can be calculated as follows:

$$\varepsilon_t = \frac{\tau\ (cot\theta/2 - a/jd)}{E_c\ (x/d - \rho_{st}) + E_s\rho_{st}} \tag{18}$$

$$\varepsilon_b = \varepsilon_{bs} = \frac{\tau\ (cot\theta/2 + a/jd)}{E_s\rho_{sb}} \tag{19}$$

where x is the neutral axis depth, a the shear span length, jd the inner level arm, E_c and E_s the Young modulus of compressive concrete and longitudinal steel rebar, respectively, and ρ_{st} and ρ_{sb} the geometrical ratio of the top and bottom longitudinal reinforcements, respectively. In the analysis, it was assumed that the beams fail at the section with the maximum bending moment and shear force.

The strain slope was obtained as $\phi = (\varepsilon_b - \varepsilon_t)/jd$, and the longitudinal strain at the centroid level was calculated as $\varepsilon_x = \varepsilon_b - \phi\ (Y_G - c)$, with Y_G and c the position of the centroid of the cross-section from bottom level and the cover thickness, respectively.

5. Iterative Procedure

After discussing all the relationships required to determine the ultimate shear, the iterative process will now be explained.

Before starting the numerical procedure, the effective strain of FRP was evaluated as suggested by Chen and Teng [21,22]. Thus, the average vertical strain at ULS was set equal to the FRP effective strain ($\varepsilon_v = \varepsilon_{fe}$). The stresses of the corroded stirrups [$\sigma_{v,c} = min(E_{sv}\ \varepsilon_v; f_{yv,c})$] and FRP ($f_{fe} = E_{fv}\ \varepsilon_v$) were obtained.

To calculate the tensile stress (σ_{c1}) and the strut inclination (θ) at ULS, a value of the principal tensile strain (σ_1) was assumed.

Then, the compression softening factor (η), the principal compressive strain ($\varepsilon_2 = \varepsilon_t\eta/2$) and concrete stress ($\sigma_{c2}$) were calculated using the stored ε_t value and Equations (13) and (14).

The tensile stress was obtained by the tension stiffening constitutive law [Equation (15)]. Its upper limit ($\sigma_{c1,max}$) depended on the crack width at ULS, which was evaluated with the stored strut angle.

The step value of θ was calculated by Equation (11). Then the ultimate shear was obtained by Equation (9).

The flexural model made it possible to check the longitudinal equilibrium at the cross-section level and the ε_t and ε_x values were also determined.

Then, by Equation (12), the new value of ε_1 was calculated and compared with the old one. The iteration process was stopped when the difference between the two values of the principal strain was less than a pre-established tolerance.

6. Validation of the Proposed Formulation and Discussion

The proposed formulation was validated against tests on RC beams reinforced in shear with FRP. To this end, an extensive literature review was carried out to collect a database of experimental results.

6.1. RC Beams with Un-Corroded Stirrups and FRP Reinforcement

The experimental campaigns of Colalillo and Sheikh [43] and Bousselham and Chaallal [44] on un-corroded specimens were used to verify the proposed model. In Table 1, the geometrical and mechanical details of the specimens, together with the calculated and experimental results, are listed. Moreover, to assess the reliability of the predictions, without taking into account overestimation or underestimation, both the Absolute Error ($AE = |V_{exp} - V_{num}|$) and the Average Absolute Error ($AAE = |V_{exp} - V_{num}|/V_{exp}$), were provided.

The formulation's capacity to calculate correctly the ultimate shear of the strengthened RC beams without any corrosion of stirrups is highlighted by the numerical results. A mean of 0.98 and a Coefficient of Variation (CoV) of 0.21 of the experimental-numerical result ratio were obtained. For the tests of Colalillo and Sheikh [43], the values *AAE* were within a range between 0.05 and 0.26, with a higher value of 0.52 for specimen S2-CA (*AE* = 454.6 kN). In contrast, for the specimens tested by Bousselham and Chaallal [44], the *AAE* is between 0,13 and 0,52.

Table 1. Experimental and numerical ultimate shear of strengthened RC beams.

Ref.	Spec.	b_w	d	f_c	f_{yv}	ρ_{sv}	f_{fu}	E_f	ρ_{fv}	W	V_{exp}	V_{num}	V_{exp}/V_{num}	AE	AAE
		mm	mm	MPa	MPa	%	MPa	GPa	%		kN	kN		kN	
[43] [1]	S0-US	400	545	53.3	501	0.00	961	95	0.25	U	377.0	395.2	0.95	18.2	0.05
	S0-UA	400	545	53.3	501	0.00	961	95	0.50	U	534.0	493.6	1.08	40.4	0.08
	S0-CS	400	545	47.6	501	0.00	961	95	0.25	C	695.0	522.2	1.33	172.8	0.25
	S0-CA	400	545	53.3	501	0.00	961	95	0.50	C	915.0	1151.8	0.79	236.8	0.26
	S5-US	400	545	47.6	501	0.07	961	95	0.25	U	518.0	480.3	1.08	37.7	0.07
	S5-UA	400	545	47.5	501	0.07	961	95	0.50	U	622.0	563.7	1.10	58.3	0.09
	S5-CS	400	545	47.6	501	0.07	961	95	0.25	C	725.0	611.1	1.19	113.9	0.16
	S2-US	400	545	47.5	501	0.14	961	95	0.25	U	629.0	703.3	0.89	74.3	0.12
	S2-UA	400	545	47.5	501	0.14	961	95	0.50	U	688.0	776.3	0.89	88.3	0.13
	S2-CS	400	545	47.5	501	0.14	961	95	0.25	C	844.0	815.5	1.03	28.5	0.03
	S2-CA	400	545	47.5	501	0.14	961	95	0.50	C	866.0	1320.6	0.66	454.6	0.52
[44] [2]	S0-0.5L-400	152	350	25.0	645	0.00	3159	243	0.08	U	102.4	138.6	0.74	36.2	0.35
	S0-1L-400	152	350	25.0	645	0.00	3159	243	0.14	U	120.0	160.2	0.75	40.2	0.33
	S0-2L-400	152	350	25.0	645	0.00	3159	243	0.28	U	122.0	189.7	0.64	67.7	0.56
	S1-0.5L-400	152	350	25.0	645	0.38	3159	243	0.08	U	282.0	323.3	0.87	41.3	0.15
	S1-2L-400	152	350	25.0	645	0.38	3159	243	0.28	U	267.2	333.2	0.80	66.0	0.25
	S0-1L-220	95	175	26.0	420	0.00	3650	231	0.14	U	59.3	51.7	1.15	7.6	0.13
	S0-2L-220	95	175	26.0	420	0.00	3650	231	0.28	U	68.5	57.7	1.19	10.8	0.16
	S1-1L-220	95	175	26.0	420	0.38	3650	231	0.14	U	95.7	78.9	1.21	16.8	0.18
	S1-2L-220	95	175	26.0	420	0.38	3650	231	0.28	U	105.1	83.0	1.27	22.1	0.21
												Mean	0.98	81.6	0.20
												CoV	0.21	1.28	0.71

[1] R-section; f_{yl} = 481 MPa; ρ_{sb} = 2.57%; and a/d = 3.07; [2] T-section; f_{yl} = 480 MPa; ρ_{sb} = 3.75%; and a/d = 3.

6.2. RC Beams with Corroded Stirrups and FRP Reinforcement

The information and experimental results on strengthened RC beams with corroded stirrups [6–8], which were used to further examine the soundness of the proposed formulation, are listed in Table 2.

As expected, with an increasing degree of corrosion of the steel stirrups (Q_c), the ultimate shear generally decreases. Adequate agreement between the calculated results and the experimental data was confirmed by a mean of 1.02 and a CoV of 0.13 of the experimental-numerical results ratio. The *AAE* ranges between 0 and 0.21 and with limited values of the *AE*.

Table 2. Experimental and numerical ultimate shear of strengthened RC beams with corroded stirrups.

Ref.	Spec.	b_w	d	f_c	f_{yv}	ρ_{sv}	Q_c	f_{fu}	E_f	ρ_{fv}	W	V_{exp}	V_{num}	V_{exp}/V_{num}	AE	AAE
		mm	mm	MPa	MPa	%	%	MPa	GPa	%		kN	kN		kN	
[6] [1]	C1-NS	300	200	32.0	344	0.33	8					98.4	85.1	1.16	13.3	0.13
	C2-NS	300	200	32.0	344	0.33	15					92.8	80.8	1.15	12.0	0.13
	C1-EB1	300	200	32.0	344	0.33	8	894	65	0.37	U	120.0	120.1	1.00	0.1	0.00
	C2-EB1	300	200	32.0	344	0.33	15	894	65	0.37	U	100.0	116.3	0.86	16.3	0.16
	C2-EB2	300	200	32.0	344	0.33	15	894	65	0.74	U	107.2	125.5	0.85	18.3	0.17
	C2-EB3	300	200	32.0	344	0.33	15	894	65	1.11	U	120.0	130.7	0.92	10.7	0.09

Table 2. *Cont.*

Ref.	Spec.	b_w	d	f_c	f_{yv}	ρ_{sv}	Q_c	f_{fu}	E_f	ρ_{fv}	W	V_{exp}	V_{num}	V_{exp}/V_{num}	AE	AAE
		mm	mm	MPa	MPa	%	%	MPa	GPa	%		kN	kN		kN	
[7] [2]	N07	260	295	30.7	542	0.29	6					148.0	134.4	1.10	13.6	0.09
	N12	260	295	30.7	542	0.29	12					155.0	126.7	1.22	28.3	0.18
	S07	260	295	30.5	542	0.29	6	986	96	1.60	U	174.0	200.2	0.87	26.2	0.15
	S12	260	295	30.5	542	0.29	12	986	96	1.60	U	174.0	198.7	0.88	24.7	0.14
[8] [3]	B1	120	165	24.6	440	0.24	1					61.2	48.3	1.27	12.9	0.21
	B2	120	165	27.3	440	0.24	3					58.2	50.0	1.16	8.2	0.14
	B3	120	165	29.1	440	0.24	4					45.0	50.8	0.89	5.8	0.13
	B4	120	165	26.0	440	0.24	5					55.0	48.1	1.14	6.9	0.12
	B5	120	165	29.8	440	0.24	7					42.5	50.4	0.84	7.9	0.19
	B6	120	165	28.9	440	0.24	7					52.0	49.5	1.05	2.5	0.05
	B7	120	165	25.6	440	0.24	10					40.0	46.1	0.87	6.1	0.15
	SB1	120	165	24.6	440	0.24	1	3060	210	0.06	U	58.1	58.5	0.99	0.4	0.01
	SB2	120	165	27.3	440	0.24	3	3060	210	0.06	U	65.0	61.2	1.06	3.8	0.06
	SB3	120	165	29.1	440	0.24	4	3060	210	0.06	U	62.5	62.6	1.00	0.1	0.00
	SB4	120	165	26.0	440	0.24	5	3060	210	0.06	U	61.1	59.1	1.03	2.0	0.03
	SB5	120	165	29.8	440	0.24	7	3060	210	0.06	U	60.0	62.6	0.96	2.6	0.04
	SB6	120	165	28.9	440	0.24	7	3060	210	0.06	U	64.0	61.5	1.04	2.5	0.04
	SB7	120	165	25.6	440	0.24	10	3060	210	0.06	U	68.8	57.2	1.20	11.6	0.17
														1.02	9.86	0.11
														0.13	0.84	0.59

[1] T-section; f_{yl} = 520 MPa; ρ_{sb} = 2.31%; and a/d = 3; [2] T-section; f_{yl} = 537 MPa; ρ_{sb} = 2.56%; and a/d = 3.05; [3] R-section; f_{yl} = 467 MPa; ρ_{sb} = 2.57%; and a/d = 2.42.

7. Parametric Analysis

A parametric analysis was carried out to investigate the influence of the key factors involved in calculating ultimate shear.

The basic numerical specimens had the same geometrical and mechanical characteristics as the SB1 (Table 2). The degree of corrosion, the cylinder compressive strength, the stirrup ratio, and the strengthening methods were changed. Then the proposed formulation was applied to calculate the ultimate shear.

7.1. Effect of Degree of Corrosion

In Figure 4, the numerical results obtained assuming a constant cylinder compressive strength of 20 MPa are shown. The use of a C wrap arrangement provided a slightly higher value of ultimate shear for each degree of corrosion considered. The ultimate shear decay between each corrosion degree considered is about 4–5%. The beams strengthened with wrapped FRP sheets fail with tensile rupture of FRP sheets, and the concrete strength has a slight influence on the ultimate shear.

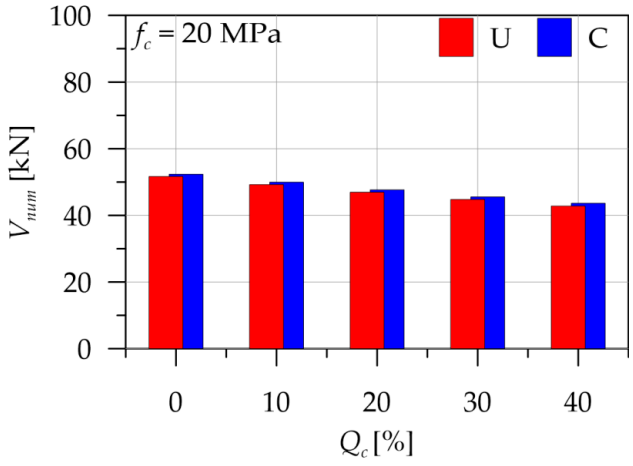

Figure 4. Effect of corrosion degree on the ultimate shear.

The decreasing trend of ultimate shear with an increase in the degree of corrosion, as expected, was very similar for both wrap arrangements considered (U, and C). Further, it is influenced by reduction of stirrups stress, which is linear with the degree of corrosion. In any case, the contributions of corroded stirrups to the ultimate shear of RC beam appears limited.

7.2. Effect of Concrete Cylinder Compressive Strength and Geometrical Stirrup Ratio

In Figure 5, the effects of concrete cylinder compressive strength and geometrical stirrup ratio on ultimate shear are plotted.

For low values of concrete cylinder compressive strength, the ultimate shear was only slightly influenced by both the degree of corrosion and the wrap arrangement. Increasing the cylinder compressive strength of concrete, the numerical specimen with a U arrangement showed a greater increase in ultimate shear with respect to the C one. Since for the former (U), besides the strength increases due to local shear strength on the crack surface (τ_i), the debonding phenomena are also delayed. Moreover, the degree of corrosion of steel stirrups has more influence on the results.

Figure 5b shows that the ultimate shear was proportionally related to the adopted value of the geometrical stirrup ratio. When an adequate amount of FRP is used in heavily corroded specimens ($Q_c \geq 20\%$), the ultimate shear is mainly ensured by the FRP reinforcement, and the geometrical stirrup ratio has little influence on the overall shear strength.

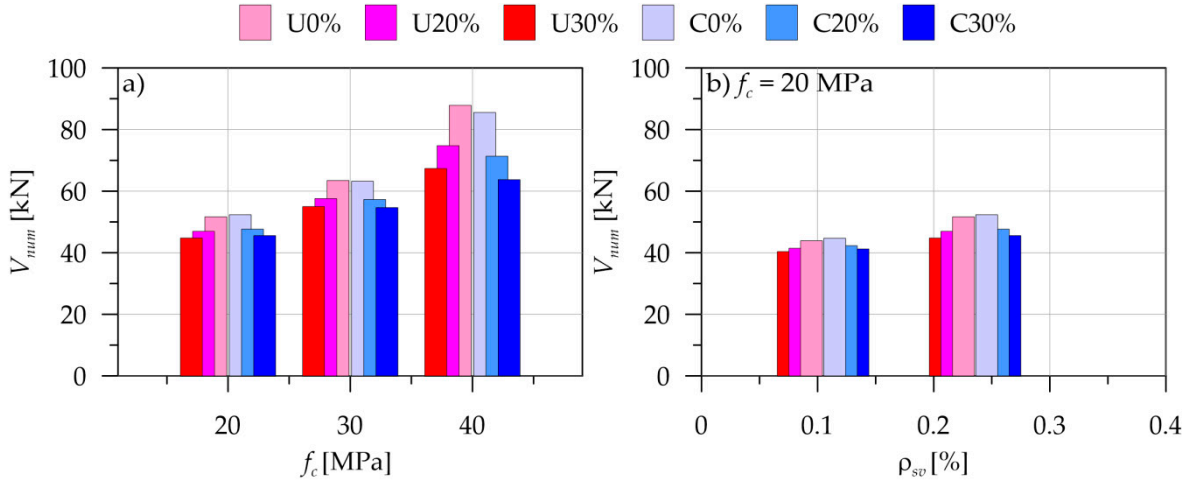

Figure 5. (**a**) Effect of cylinder compressive strength and (**b**) geometrical stirrup ratio on ultimate shear for different corrosion degrees.

8. Conclusions

In this paper, an analytical formulation for predicting the ultimate shear of RC beams with corroded stirrups and strengthened with FRP is presented.

The proposed procedure for ultimate shear takes into account both the shear and flexural models. The basic equations of the MCFT were used to calculate an equilibrated and compatible solution at ULS.

Both debonding and tensile stress rupture of FRP reinforcement were adequately considered.

The effect of stirrup corrosion was taken into account by using an empirical formulation previously proposed by the same authors. It was found to be very suitable to calculate the contribution of stirrups to ultimate shear.

The proposed formulation was validated against experimental results collected in the literature. First, two sets of specimens reinforced with FRP were used to verify the ability of the model to predict ultimate shear value in the case of un-corroded specimens. Then the model was applied to three sets of data involving specimens with corroded stirrups and reinforced in shear with FRP.

In both cases, the proposed model provided enough numerical results, especially for the case of corroded RC beams also using a simple formulation, to reproduce the steel yield strength decay due to the corrosion phenomena. Of course, a more detailed representation of the corrosion damage, also involving the diameter of stirrups as variable, could refine the numerical results

With the aim of exploring the influence of some key parameters, an extensive numerical analysis was carried out. The effects of degree of corrosion, concrete cylinder compressive strength, geometrical stirrup ratio and wrap arrangement were investigated.

As expected, an increase in the degree of corrosion caused a decrease in the ultimate shear for each kind of wrap arrangement considered.

Ultimate shear was influenced more by the degree of stirrup corrosion on specimens with low values of concrete cylinder compressive strength.

Author Contributions: N.S., P.C., A.R. and F.T. made equal contributions to all the actions necessary for the realization of the paper.

Funding: This research was funded by "MIUR–Ministero dell'Istruzione, dell'Università e della Ricerca" grant number "PRIN 2015HZ24KH" ("Failure mechanisms caused by corrosive degrade and by lack of constructive details in the existing structures in reinforced concrete."). The first author wishes to express his personal gratitude to this fund, through which a research fellow scholarship was awarded.

Conflicts of Interest: The authors declare no conflict of interest.

Nomenclature

AAE	Average Absolute Error
AE	Absolute error
A_f	Area of the FRP reinforcement
A_{sv}, $A_{sv,c}$	Area of non corroded and corroded stirrup
a	Shear span
b_w, h, d	Width, height and effective depth of the cross-section
c	Concrete cover
C, T	Resultant forces in the concrete and the steel rebar related to the i-th layer
d_f	Depth of FRP reinforcement
d_g	Maximum coarse aggregate size (in mm)
E_c, E_f, E_s	Young modulus of concrete, FRP and steel
f_c, f_{ct}	Peak compressive stress of concrete and tensile strength of concrete
f_{yl}	Yield strength of longitudinal steel rebar
f_{yv}, $f_{yv,c}$	Yield strength of non corroded and corroded steel stirrup
jd	Inner lever arm
N, M, V	Axial force, bending moment and shear force
R_{fr}, R_{fd}	Rupture and debonding effectiveness factors
s_v	Stirrups spacing
s_f, t_f, w_f	Spacing, thickness, and width of FRP sheets
S_m, S_{ml}, S_{mv}	Average crack spacing
w	Shear crack width
W	Wrap arrangement (S, U, or C)
x	Neutral axis depth
ε_1, ε_2	Principal strains
ε_b, ε_t	Bottom and top longitudinal force strain
ε_{cb}, ε_{ct}	Bottom and top longitudinal concrete strain
ε_{c0}	Concrete strain at the peak compressive stress
ε_{fe}, ε_{fu}	Effective and nominal ultimate strain of FRP

ε_x	Axial strain at centroid level
ε_v	Average vertical strain
η	Compression softening factor
θ	Crack angle
ρ_{fv}, $\rho_{sv,c}$	Geometrical ratio of FRP and corroded stirrup reinforcement
ρ_{sb}, ρ_{st}	Geometrical ratio of bottom and top longitudinal rebar
ϕ	Curvature
σ_{c1}, σ_{c2}	Principal stresses
σ_{c1max}	Maximum principal tensile stress
σ_{cv}	Clamping stresses
σ_{fv}, $\sigma_{sv,c}$, σ_{sl}	Stress of FRP, corroded stirrups and longitudinal rebars
τ, τ_i	Shear stress and local shear stress on the crack surface

References

1. Colajanni, P.; Recupero, A.; Ricciardi, G.; Spinella, N. Failure by corrosion in PC bridges: A case history of a viaduct in Italy. *Int. J. Struct. Integr.* **2016**, *7*, 181–193. [CrossRef]
2. Presti, A.L.; Recupero, A.; Spinella, N. Influence of rebar corrosion on RC frame push-over response. In Proceedings of the High Tech Concrete: Where Technology and Engineering Meet—2017 Fib Symposium, Maastricht, The Netherlands, 12–14 June 2017; pp. 2118–2126.
3. Cesetti, A.; Mancini, G.; Tondolo, F.; Recupero, A.; Spinella, N. Physical model for structural evaluation of R.C. beams in presence of corrosion. In Proceedings of the 4th International Conference on Concrete Repair, Rehabilitation and Retrofitting (ICCRRR 2015), Leipzig, Germany, 5–7 October 2016; pp. 107–114.
4. Rodriguez, J.; Ortega, L.M.; Casal, J.; Diez, J.M. Assessing structural conditions of concrete structures with corroded reinforcement. In Proceedings of the Conference, Concrete Repair, Rehabilitation and Protection, Dundee, UK, 24–26 June 1996; E & FN Spon: Dundee, UK, 1996; pp. 65–78.
5. Bossio, A.; Fabbrocino, F.; Monetta, T.; Lignola, G.P.; Prota, A.; Manfredi, G.; Bellucci, F. Corrosion effects on seismic capacity of reinforced concrete structures. *Corros. Rev.* **2018**. [CrossRef]
6. El-Maaddawy, T.; Chekfeh, Y. Shear Strengthening of T-Beams with Corroded Stirrups Using Composites. *ACI Struct. J.* **2013**, *110*, 779–790.
7. Qin, S.; Dirar, S.; Yang, J.; Chan, A.H.C.; Elshafie, M. CFRP Shear Strengthening of Reinforced-Concrete T-Beams with Corroded Shear Links. *J. Compos. Constr.* **2015**, *19*, 04014081. [CrossRef]
8. Li, H.; Wu, J.; Wang, Z. Shear Performance of Reinforced Concrete Beams with Corroded Stirrups Strengthened with Carbon Fiber-Reinforced Polymer. *ACI Struct. J.* **2016**, *113*, 51–61. [CrossRef]
9. Mosallam, A.S.; Banerjee, S. Shear enhancement of reinforced concrete beams strengthened with FRP composite laminates. *Compos. Part B Eng.* **2007**, *38*, 781–793. [CrossRef]
10. Val, D.V. Deterioration of Strength of RC Beams due to Corrosion and Its Influence on Beam Reliability. *J. Struct. Eng.* **2007**, *133*, 1297–1306. [CrossRef]
11. Recupero, A.; Spinella, N.; Tondolo, F. A model for the analysis of ultimate capacity of RC and PC corroded beams. *Adv. Civ. Eng.* **2018**. [CrossRef]
12. Recupero, A.; Spinella, N.; Tondolo, F. Failure analysis of corroded RC beams subjected to shear-flexural actions. *Eng. Fail. Anal.* **2018**. [CrossRef]
13. Zhang, W.; Ye, Z.; Gu, X. Effects of stirrup corrosion on shear behaviour of reinforced concrete beams. *Struct. Infrastruct. Eng.* **2017**, *13*, 1081–1092. [CrossRef]
14. Campione, G.; Cannella, F. Engineering failure analysis of corroded R.C. beams in flexure and shear. *Eng. Fail. Anal.* **2018**, *86*, 100–114. [CrossRef]
15. Colajanni, P.; La Mendola, L.; Recupero, A.; Spinella, N. Stress field model for strengthening of shear-flexure critical RC beams. *J. Compos. Constr.* **2017**, *21*. [CrossRef]
16. Marí, A.; Cladera, A.; Oller, E.; Bairán, J. Shear design of FRP reinforced concrete beams without transverse reinforcement. *Compos. Part B Eng.* **2014**, *57*, 228–241. [CrossRef]

17. Triantafyllou, G.G.; Rousakis, T.C.; Karabinis, A.I. Analytical assessment of the bearing capacity of RC beams with corroded steel bars beyond concrete cover cracking. *Compos. Part B Eng.* **2017**, *119*, 132–140. [CrossRef]
18. Alabdulhady, M.Y.; Aljabery, K.; Sneed, L.H. Analytical Study on the Torsional Behavior of Reinforced Concrete Beams Strengthened with FRCM Composite. *J. Compos. Constr.* **2019**, *23*, 04019006. [CrossRef]
19. Elghazy, M.; El Refai, A.; Ebead, U.; Nanni, A. Experimental results and modelling of corrosion-damaged concrete beams strengthened with externally-bonded composites. *Eng. Struct.* **2018**, *172*, 172–186. [CrossRef]
20. Vecchio, F.J.; Collins, M.P. The Modified Compression-Field Theory for Reinforced Concrete Elements Subjected to Shear. *ACI J. Proc.* **1986**, *83*, 219–231.
21. Chen, J.F.; Teng, J.G. Shear capacity of FRP-strengthened RC beams: FRP debonding. *Constr. Build. Mater.* **2003**, *17*, 27–41. [CrossRef]
22. Chen, J.F.; Teng, J.G. Shear Capacity of Fiber-Reinforced Polymer-Strengthened Reinforced Concrete Beams: Fiber Reinforced Polymer Rupture. *J. Struct. Eng.* **2003**, *129*, 615–625. [CrossRef]
23. Cairns, J.; Plizzari, G.A.; Du, Y.; Law, D.W.; Franzoni, C. Mechanical Properties of Corrosion-Damaged Reinforcement. *ACI Mater. J.* **2005**, *102*, 256–264.
24. Cobo, A.; Moreno, E.; Cánovas, M.F.; Cánovas, M.F. Mechanical properties variation of B500SD high ductility reinforcement regarding its corrosion degree. *Mater. Construcción* **2011**, *61*, 517–532.
25. Zhang, W.; Song, X.; Gu, X.; Li, S. Tensile and fatigue behavior of corroded rebars. *Constr. Build. Mater.* **2012**, *34*, 409–417. [CrossRef]
26. Apostolopoulos, C.A.; Demis, S.; Papadakis, V.G. Chloride-induced corrosion of steel reinforcement – Mechanical performance and pit depth analysis. *Constr. Build. Mater.* **2013**, *38*, 139–146. [CrossRef]
27. Fernandez, I.; Bairán, J.M.; Marí, A.R. Mechanical model to evaluate steel reinforcement corrosion effects on σ–ε and fatigue curves. Experimental calibration and validation. *Eng. Struct.* **2016**, *118*, 320–333. [CrossRef]
28. Imperatore, S.; Rinaldi, Z.; Drago, C. Degradation relationships for the mechanical properties of corroded steel rebars. *Constr. Build. Mater.* **2017**, *148*, 219–230. [CrossRef]
29. Zhu, W.; François, R.; Cleland, D.; Coronelli, D. Failure mode transitions of corroded deep beams exposed to marine environment for long period. *Eng. Struct.* **2015**, *96*, 66–77. [CrossRef]
30. Biondini, F.; Vergani, M. Deteriorating beam finite element for nonlinear analysis of concrete structures under corrosion. *Struct. Infrastruct. Eng.* **2015**, *11*, 519–532. [CrossRef]
31. Colalillo, M.A.; Sheikh, S.A. Behavior of Shear-Critical Reinforced Concrete Beams Strengthened with Fiber-Reinforced Polymer—Analytical Method. *ACI Struct. J.* **2014**, *111*, 1385–1396. [CrossRef]
32. Mostafaei, H.; Vecchio, F.J. Uniaxial Shear-Flexure Model for Reinforced Concrete Elements. *J. Struct. Eng.* **2008**, *134*, 1538–1547. [CrossRef]
33. Colajanni, P.; La Mendola, L.; Mancini, G.; Recupero, A.; Spinella, N. Shear capacity in concrete beams reinforced by stirrups with two different inclinations. *Eng. Struct.* **2014**, *81*, 444–453. [CrossRef]
34. Baghi, H.; Barros, J.A.O.; Menkulasi, F. Shear strengthening of reinforced concrete beams with Hybrid Composite Plates (HCP) technique: Experimental research and analytical model. *Eng. Struct.* **2016**, *125*, 504–520. [CrossRef]
35. Rousakis, T.C.; Saridaki, M.E.; Mavrothalassitou, S.A.; Hui, D. Utilization of hybrid approach towards advanced database of concrete beams strengthened in shear with FRPs. *Compos. Part B Eng.* **2016**, *85*, 315–335. [CrossRef]
36. Yapa, H.D.; Lees, J.M. Rectangular Reinforced Concrete Beams Strengthened with CFRP Straps. *J. Compos. Constr.* **2014**, *18*, 04013032. [CrossRef]
37. Sigrist, V. Generalized Stress Field Approach for Analysis of Beams in Shear. *ACI Struct. J.* **2011**, *108*, 479–487.
38. CEN Eurocode 2—Design of Concrete Structures: Part 1–1. General Rules and Rules for Buildings. CEN (Comitee for Standardization) 1992-1-1. 2005.
39. Italian MIT, D.M. Nuove Norme Tecniche Per le Costruzioni. *Gazzetta Ufficiale*, 14 January 2008; Volume 29. (In Italian)
40. Bentz, E.C.; Vecchio, F.J.; Collins, M.P. Simplified Modified Compression Field Theory for Calculating Shear Strength of Reinforced Concrete Elements. *ACI Struct. J.* **2006**, *103*, 614–624.

41. Colajanni, P.; Papia, M.; Spinella, N. Stress-strain law for confined concrete with hardening or softening behavior. *Adv. Civ. Eng.* **2013**, *2013*. [CrossRef]
42. Spinella, N. N-M-χ interaction for arbitrary cross section under biaxial bending and axial load. *Pollack Period.* **2013**, *8*, 87–100. [CrossRef]
43. Colalillo, M.A.; Sheikh, S.A. Behavior of Shear-Critical Reinforced Concrete Beams Strengthened with Fiber-Reinforced Polymer—Experimentation. *ACI Struct. J.* **2014**, *111*, 1373–1384. [CrossRef]
44. Bousselham, A.; Chaallal, O. Behavior of Reinforced Concrete T-Beams Strengthened in Shear with Carbon Fiber-Reinforced Polymer— An Experimental Study. *ACI Struct. J.* **2006**, *103*, 339–347.

© 2019 by the authors. Licensee MDPI, Basel, Switzerland. This article is an open access article distributed under the terms and conditions of the Creative Commons Attribution (CC BY) license (http://creativecommons.org/licenses/by/4.0/).